


Communication

Broadband Detection Based on 2D Bi₂Se₃/ZnO Nanowire Heterojunction

Zhi Zeng^{1,2}, Dongbo Wang^{1,2,*} , Jinzhong Wang^{1,2,*}, Shujie Jiao^{1,2,*}, Donghao Liu^{1,2}, Bingke Zhang^{1,2}, Chenchen Zhao^{1,2}, Yangyang Liu^{1,2}, Yaxin Liu^{1,2}, Zhikun Xu^{3,4,*}, Xuan Fang^{5,*} and Liancheng Zhao^{1,2}

¹ National Key Laboratory for precision Hot Processing of Metals, Harbin Institute of Technology, Harbin 150001, China; zengzhi@hit.edu.cn (Z.Z.); 19s009009@stu.hit.edu.cn (D.L.); 18S009003@stu.hit.edu.cn (B.Z.); 20b909059@stu.hit.edu.cn (C.Z.); 20s009008@stu.hit.edu.cn (Y.L.); 20s009004@stu.hit.edu.cn (Y.L.); lczhao@hit.edu.cn (L.Z.)

² Department of Optoelectronic Information Science, Harbin Institute of Technology, School of Materials Science and Engineering, Harbin 150001, China

³ College of Science, Guangdong University of Petrochemical Technology, Maoming City 525000, China

⁴ Key Laboratory for Photonic and Electronic Bandgap Materials, Ministry of Education, School of Physics and Electronic Engineering, Harbin Normal University, Harbin 150025, China

⁵ State Key Laboratory of High Power Semiconductor Lasers, School of Science, Changchun University of Science and Technology, Changchun 130022, China

* Correspondence: wangdongbo@hit.edu.cn (D.W.); jinzhong_wang@hit.edu.cn (J.W.); shujiejiao@hit.edu.cn (S.J.); xuzhikun@gdupt.edu.cn (Z.X.); fangx@cust.edu.cn (X.F.)



Citation: Zeng, Z.; Wang, D.; Wang, J.; Jiao, S.; Liu, D.; Zhang, B.; Zhao, C.; Liu, Y.; Liu, Y.; Xu, Z.; et al. Broadband Detection Based on 2D Bi₂Se₃/ZnO Nanowire Heterojunction. *Crystals* **2021**, *11*, 169. <https://doi.org/10.3390/cryst11020169>

Academic Editors:

Alessandro Chiasera and

Aleksej Zarkov

Received: 10 December 2020

Accepted: 1 February 2021

Published: 8 February 2021

Publisher's Note: MDPI stays neutral with regard to jurisdictional claims in published maps and institutional affiliations.



Copyright: © 2021 by the authors. Licensee MDPI, Basel, Switzerland. This article is an open access article distributed under the terms and conditions of the Creative Commons Attribution (CC BY) license (<https://creativecommons.org/licenses/by/4.0/>).

Abstract: The investigation of photodetectors with broadband response and high responsivity is essential. Zinc Oxide (ZnO) nanowire has the potential of application in photodetectors, owing to the great optoelectrical property and good stability in the atmosphere. However, due to a large number of nonradiative centers at interface and the capture of surface state electrons, the photocurrent of ZnO based photodetectors is still low. In this work, 2D Bi₂Se₃/ZnO NWAs heterojunction with type-I band alignment is established. This heterojunction device shows not only an enhanced photoresponsivity of 0.15 A/W at 377 nm three times of the bare ZnO nanowire (0.046 A/W), but also a broadband photoresponse from UV to near infrared region has been achieved. These results indicate that the Bi₂Se₃/ZnO NWAs type-I heterojunction is an ideal photodetector in broadband detection.

Keywords: 2D Bi₂Se₃/ZnO NWAs heterojunction; broadband detection; ZnO NWAs; UV detection

1. Introduction

Over the past decades, photodetectors have been extensively used in both military and civil fields, such as living cell inspection [1], night vision [2], optical communications [3], atmospheric [4], etc. [5–8]. Photodetectors have become indispensable in daily life. Among these semiconductor materials for making photodetectors, ZnO has the potential of application in UV photodetectors. Owing to the great optoelectrical property and good stability in the atmosphere, ZnO is widely researched with the band gap of 3.37 eV, of which brought by high exciton binding energy (60 meV) at room temperature, noise interference is suppressed. In addition, the merits of being low-cost, non-toxic and easy to prepare make it more attractive to be investigated [9–11]. Various morphologies of ZnO have been prepared during years of research, such as nanoparticle, nanowire, nanotube, nanofilm, and nanosheet [12–15]. The morphology with different dimensions has different characteristics. With the morphology of one-dimensional nanowire arrays (NWAs), not only the space between the nanowire is well backed up for the strengthening of light trapping ability but also the superior transport properties provide the fast electron transport channel when making comparisons with its bulk and thin-film structures [16,17].

However, until now, the photoresponse performance of the ZnO nanowires UV detector is still lower than the theoretical predicted value, due to a large number of nonradiative centers at interface and electron trapped by the surface states [18].

Many methods have been used to optimize the performance of the ZnO nanowires UV photodetector (UVPD). Yang et al. reported photocurrent enhanced through optimizing ZnO seed layer growth condition [19]. Research of Kim et al. shows that NiO/Ni coated ZnO NWs reveal raised D0X transition due to the increasing oxygen deficiency which is responsible for increasing donor density [20]. Zhang et al. reported a two-dimensional graphene/ZnO nanowire mixed-dimensional van der Waals heterostructure for high-performance photosensing [21]. Zang et al. reported enhancing photoresponse based on ZnO nanoparticles decorated CsPbBr₃ films [22]. Sumesh et al. reported broadband and highly sensitive photodetector based on ZnO/WS₂ heterojunction [23]. So far, more and more two-dimensional materials/ZnO nanowires mixed dimensional heterojunctions have been reported [24–27].

Up to now, as the discovery of the unique characteristic of topological insulators (TI), further attention is paid to TI to fabricate photodetectors [28–31]. Taking advantage of Dirac dispersion and spin-momentum locking property brought by 2D surface electrons and time-reversal symmetry, back scattering in the Dirac fermions caused by nonmagnetic impurities is prevented, which enable the outstanding transport characteristics, thus reducing the dark current to obtain higher performance [32]. With direct band gap of 0.3 eV and weak Van der Waals' force between each two layers, Bi₂Se₃ has very infusive photoelectric properties, such as tunable surface bandgap, polarization-sensitive photocurrent, and thickness dependent optical absorption [33,34]. These special properties make Bi₂Se₃ promise for binding with ZnO to build high performance photodetector in the UV and visible region. In contrast, there are scarcely any reports about 2D Bi₂Se₃/ZnO nanowire mixed-dimensional detectors.

In this work, hydrothermal synthesized ZnO NWAs is composite with 2D Bi₂Se₃. The broadband photodetector based on Bi₂Se₃/ZnO NWAs heterojunction photodetector is fabricated. Enhanced UV to visible responsivity is realized in the Bi₂Se₃/ZnO NWAs heterojunction photodetector. The mechanism of enhanced response in Bi₂Se₃/ZnO NWAs heterojunction is dealt with in detail through thorough inspections of photoelectric response characteristic combined with Raman scattering measurements, optical properties, and band gap structure.

2. Materials and Methods

2.1. Syntheses of ZnO NWAs

ZnO NWAs were synthesized via a simple hydrothermal method with buffer layer sputtered on fluorine-doped tin oxide (FTO) glass. A thin buffer layer was deposited with RF magnetron sputtering, during which process, the O₂:Ar flow ratio was controlled at 18:42 in 1 Pa under room temperature for 5 min, after which, it was annealed at 400 °C for 1 h. On the basis of buffer layer, an ordinary hydrothermal method was applied for the synthesis of ZnO nanowire. Zn(AC)₂·6H₂O and C₆H₁₂N₄ (HMT) with an equal amount of 0.0009 mol were added to 30 mL deionized water and stirred for 5 min, respectively. Subsequently, the two aqueous solutions were mixed and stirred for 5 min. Then, the obtained solution was sealed in autoclave at 90 °C for 4 h. Afterwards, synthesized sample was washed with deionized water several times and dried in the air. In this way, ZnO NWAs was prepared.

2.2. Syntheses of 2D Bi₂Se₃

2D Bi₂Se₃ is provided in SixCarbon Technology Shenzhen.

2D Bi₂Se₃ was synthesized via a standard chemical vaporous deposition method. The reactions were conducted in a tube furnace with dual heating zone. 0.1 g 99.995% Bi₂O₃ (Bi₂O₃, 6CARBON, Shenzhen, Guangzhou, China) powder was placed in the high temperature zone to heat up to 700 degrees. 0.5 g 99.999% purity Se (Se, 6CARBON,

Shenzhen, Guangzhou, China) particles were placed in the low temperature zone to heat up to 300 degrees. Under mixed carrier gas of argon and hydrogen at flow rates of 200 sccm and 15 sccm, respectively, the clean sapphire film placed 5 cm below Bi_2O_3 was heated to 500 degrees for 15 min.

2.3. The Transfer of 2D Bi_2Se_3

Methyl methacrylate (PMMA) was coated on obtained 2D Bi_2Se_3 . After curing, PMMA was placed in pure water and heated to 90 degrees for 1 h. Then, it was quickly plunged into ice water to separate Bi_2Se_3 which attached to PMMA from sapphire base. Then, the film was placed on ZnO NWAs and finally PMMA was removed with acetone to obtain the transferred Bi_2Se_3 film.

2.4. Characterization

The morphologies of ZnO NWAs and Bi_2Se_3 film were conducted on a field-emission scanning electron microscopy (FE-SEM, ZEISS Merlin Compact, Oberkochen, Germany). Surface morphologies of Bi_2Se_3 film were also characterized by atomic force microscopy (AFM, Dimension Fastscan, Bruker, Billerica, MA, USA). Raman were carried out on (LabRAM HR Evolution, Horiba, Paris, France) with an excitation wavelength of 532 nm. Photoluminescence (PL) spectrums were recorded in CCD using the same instrument system with Raman by He–Cd laser line of 325 nm with fixed excitation intensity at room temperature. Both measurement of PL and Raman use the same equipment. The responsivity of samples was investigated by Zolix responsivity measurement system (DSR600, Zolix, Beijing, China), which calibrated via standard silicon cells. The spectral responsivity was measured in terms of the current signal within the range of 300–1000 nm at 4 V bias under room temperature.

3. Results

Figure 1a shows the dramatic structure of the photodetector. Bi_2Se_3 is transferred onto the ZnO nanowires and then onto a steam plate with platinum electrodes. The morphologies of ZnO NWAs and 2D Bi_2Se_3 were further confirmed through SEM and AFM exhibited in Figures S1 and S2 (Supplementary Materials). Due to stress and other reasons, the Bi_2Se_3 split into several pieces after the transfer. The photodetector is made by the standard semiconductor fabrication techniques. The interdigital metal electrodes, which are defined on a 300 nm Pt layer by the conventional UV photolithography and lift-off procedure, are 0.5 mm long and 300 μm wide, with a 200 μm gap. There were 10 fingers in our interdigital structure, 5 up and 5 down [35], and Figure 1b is a physical image of the detector.

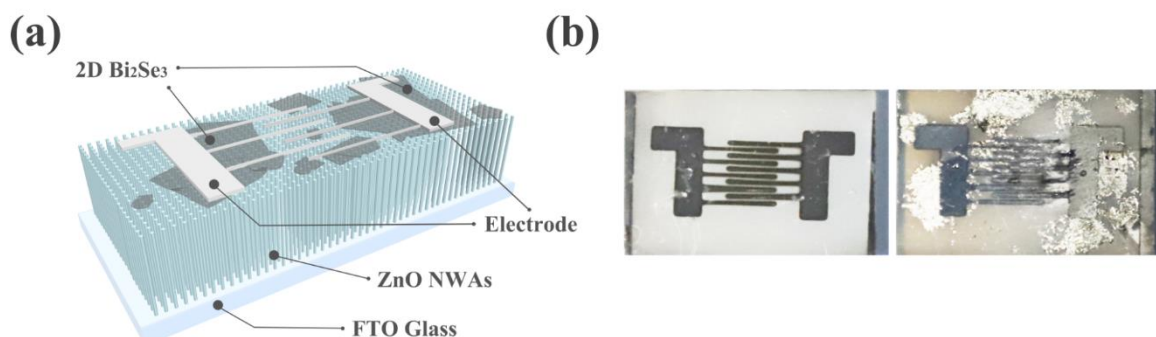


Figure 1. (a) the structure diagram and (b) physical image of photodetector.

As a widely used non-damaged measurement, Raman spectroscopy could be used to investigate intralayer vibration modes, interlayer vibration modes, and the layer coupling in 2D materials effectively [36,37]. Figure 2 showed Raman curves of ZnO NWs, 2D Bi_2Se_3 and $\text{Bi}_2\text{Se}_3/\text{ZnO}$ NWAs. Ascribed to the perpendicular laser incident direction relative to

the c-axis of sample surface, there were only two peaks located in 100 cm^{-1} and 438 cm^{-1} corresponding to E_2^{low} mode and E_2^{high} mode of ZnO NWAs in curve (a), respectively, in which the strong E_2^{high} phonon mode peak was observed, indicating the good crystalline quality [38–40]. Located at 72.8 cm^{-1} , 133.3 cm^{-1} and 174.6 cm^{-1} , three peaks observed in curve (b) could be assigned to A_{1g}^1 , E_g^2 and A_{1g}^2 vibrational mode in turn for Bi_2Se_3 [41]. A_{1g} modes were out of plane vibrations and E_g modes were vibrations in-plane [42]. There were two peaks of ZnO NWAs and one peak of Bi_2Se_3 making their appearance in curve (c), exhibiting the consistent material nature after compositing.

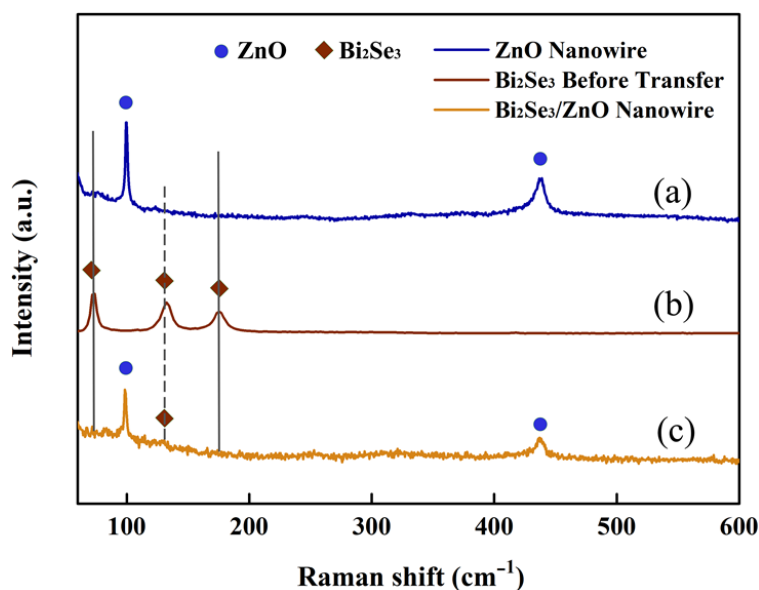


Figure 2. Raman curves of (a) ZnO NWAs, (b) 2D Bi_2Se_3 and (c) $\text{Bi}_2\text{Se}_3/\text{ZnO}$ NWAs.

Furthermore, it can be seen in Figure 2, after being transferred onto the ZnO nanowires, the Bi_2Se_3 mode slightly shifts from 133.3 cm^{-1} to the lower frequency 132 cm^{-1} corresponding to the 2D Bi_2Se_3 . This can be ascribed to the effect of residual stress [43]. The magnitude of the stress can be given by the following formula $\varepsilon = \Delta\omega/\chi$, where χ is the shift rates of Raman vibrational modes. Based on the previous literature reports, the shift rates of E_g^2 mode under biaxial strain is $\sim 5.2\text{ cm}^{-1}$ per % strain [43,44]. Therefore, the stress in the heterojunction should be 0.25%.

Since the photoluminescence characteristic could give an index to the degree of electron and hole recombination of different materials, PL test was carried out on ZnO NWAs and $\text{Bi}_2\text{Se}_3/\text{ZnO}$ NWAs to find out the change after the heterojunction forming in Figure 3. The sharp emission peak of ZnO NWAs with high intensity at 377 nm derived from near band-edge emissions [45]. In contrast, caused by oxygen vacancies [46] and chemisorbed O_2 in the air [47,48], the peak emerging at the visible region is relatively weak, suggesting the high crystal quality. The PL spectrum of $\text{Bi}_2\text{Se}_3/\text{ZnO}$ NWAs presents an obvious decrease in near band-edge emissions peak in ZnO NWAs, indicating the weakened electron hole recombination. The anomalous decreased PL emission mainly originated from the more efficient separation of photogenerated carriers at the strain-tailored heterointerfaces [43]. In the test of photoluminescence spectrum, we found that ZnO interband luminescence peaks also moved significantly, from 377 nm of simple ZnO nanowires to 378 nm of heterojunctions, which was caused by the band changes brought by stress, according to the relevant literature reports [43]. In the visible light part, the luminous emission peak shifts from 550 nm to 510 nm . It is believed that the radiant peak at 510 nm could be ascribed to the emission of Bi_2Se_3 [49]. Furthermore, it can be found that after composition with Bi_2Se_3 , the luminescence in the visible region is significantly enhanced, combining with the analysis of the $\text{Bi}_2\text{Se}_3/\text{ZnO}$ NWAs heterojunction energy

band structure below. It can be deduced that Bi_2Se_3 and ZnO form a type-I band structure, leading to the transfer of photogenerated electrons from ZnO to Bi_2Se_3 . This electron transport process results in the reduction of ZnO emission and the enhancement of Bi_2Se_3 emission. This will be discussed in detail in the energy band section.

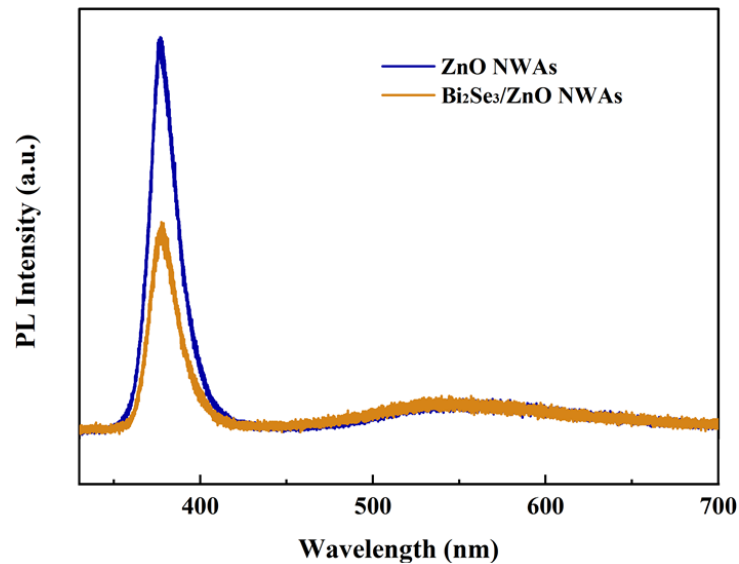


Figure 3. Photoluminescence (PL) spectra of ZnO NWAs and $\text{Bi}_2\text{Se}_3/\text{ZnO}$ NWAs.

To assess the photoresponse performance of $\text{Bi}_2\text{Se}_3/\text{ZnO}$ NWAs heterojunction, Pt interdigital electrode was sputtered with a mask to fabricate photodetector, as depicted in Figure 1. Responsivity performance is measured as shown in Figure 4. The spectral responsivity was measured in terms of the current signal in the range of 300–1000 nm at 4 V bias. All the samples revealed UV photoresponse with a cutoff wavelength of 365 nm. This can be attributed to the response of ZnO nanowires. After being transferred with the Bi_2Se_3 , the response of ZnO nanowires enhanced from 0.046 AW^{-1} to 0.15 AW^{-1} , three times higher than the bare ZnO nanowires. Furthermore, the photocurrent of $\text{Bi}_2\text{Se}_3/\text{ZnO}$ NWAs at visible and near-infrared regions is also increased compared with bare ZnO NWAs. The spectral responses in the visible and near infrared regions are from Bi_2Se_3 , corresponding to the band gap and PL spectrum of Bi_2Se_3 [50]. The performance of ordinary photodetectors constructed by nanowire and transferred 2D material could be restricted to a large extent. It is difficult to obtain effective responsivity promotion for them as the result of high interface impedance brought by impurity introduced during transfer and the limited contact area between materials of one and two dimensions. Therefore, the performance could be restricted to a large extent. In contrast, the threefold increase responsiveness of the $\text{Bi}_2\text{Se}_3/\text{ZnO}$ NWAs photodetector shows it is superior to similar detectors owing to the repressed back scattering caused by the intrinsic characteristic of TI [32,51]. In addition, the spectral test shows that the heterojunction not only significantly improves the photoelectric response in the ultraviolet region but also has good spectral response in the visible to near-infrared region, indicating that the heterojunction device has the ability to prepare wide-spectrum detectors.

For ZnO based optoelectronic devices, oxygen molecules adsorbed on the surface of the ZnO nanowires capture the free electrons, due to the surface adsorption and desorption. Therefore, a depletion layer with low conductivity is created near the surface of the film, and results in a reduced photocurrent [52,53].

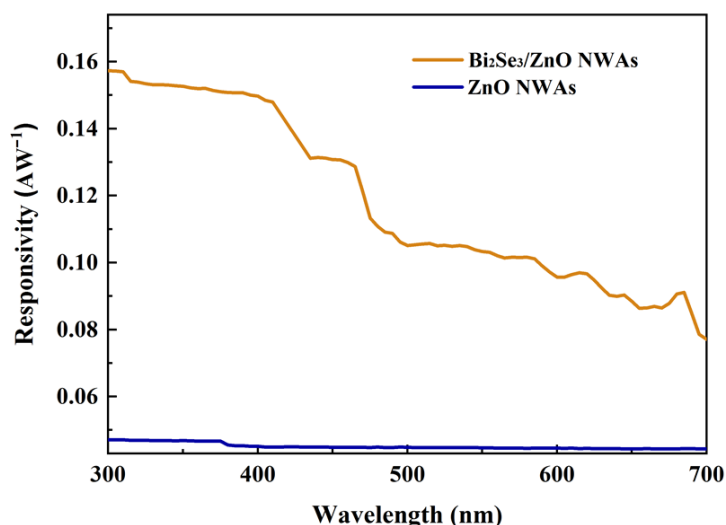


Figure 4. Responsivity spectrum of ZnO NWAs and $\text{Bi}_2\text{Se}_3/\text{ZnO}$ NWAs photodetector.

In order to study the enhance response mechanism of $\text{Bi}_2\text{Se}_3/\text{ZnO}$ NWAs heterojunctions, the energy band structure of heterojunctions is analyzed. For the heterojunction, band alignment also plays a crucial role in the spectral response characteristics [54].

The band structure of $\text{Bi}_2\text{Se}_3/\text{ZnO}$ can be deduced from the Anderson model shown in Figure 5 [55,56]. Based on previously reported energy band data of Bi_2Se_3 and ZnO [33,34,43,49,50,52,57,58], the conduction band offset (CBO) of the $\text{Bi}_2\text{Se}_3/\text{ZnO}$ heterojunction is worked out to be 1.67 ± 0.15 eV. With this band alignment, electrons can easily drift from ZnO to the Bi_2Se_3 . As a result, the recombination of electrons and holes may mainly take place on the Bi_2Se_3 side rather than in ZnO nanowires. This will mitigate the impact of the ZnO surface adsorption and desorption. Hence, at the same time of leading to an increase in the UV current of the $\text{Bi}_2\text{Se}_3/\text{ZnO}$ NWAs heterojunction, the drifting of electrons also results in a decrease of ZnO emission in the UV region. In this way, the realization of $\text{Bi}_2\text{Se}_3/\text{ZnO}$ NWAs heterojunction photodetectors makes responsivity of $\text{Bi}_2\text{Se}_3/\text{ZnO}$ NWAs improve noticeably in the UV region, however, the absorption range broadened effectively.

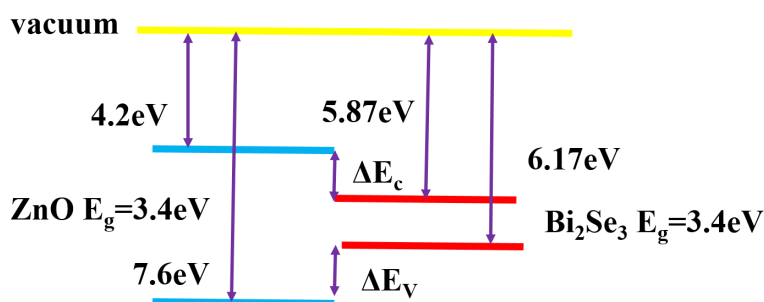


Figure 5. Electronic band alignment for $\text{Bi}_2\text{Se}_3/\text{ZnO}$ NWAs structure.

4. Conclusions

In summary, this work presents a novel broadband heterojunction photodetector based on 2D $\text{Bi}_2\text{Se}_3/\text{ZnO}$ NWAs. Combining the merit of 2D Bi_2Se_3 and ZnO, the responsivity spectrum of the photodetector exhibited the improved responsivity covering UV-Visible-Near Infrared range. The properties of a responsivity of 0.15 A/W, nearly three times to the bare ZnO, benefit from unique advantages of type-I band alignments. More importantly, the special heterojunction photodetector with type-I energy band structure injects a large number of electrons into the ultrathin 2D material to enhance responsivity of Visible-Near

Infrared wavelength while exporting electrons to the electrode rapidly to avoid electron and hole recombination, making it a promising and yet-to-be-extended way for novel exploration for more applications.

Supplementary Materials: The following are available online at <https://www.mdpi.com/2073-4352/11/2/169/s1>, Figure S1: (a) low magnification and (b) high magnification SEM images of ZnO NWAs; (c) low magnification and (d) high magnification SEM images of Bi₂Se₃; Figure S2: (a) 2D and (b) 3D AFM images of Bi₂Se₃.

Author Contributions: Conceptualization, J.W.; methodology, B.Z., Y.L. (Yaxin Liu), and C.Z.; formal analysis, D.W. and Z.Z.; investigation, D.L.; data curation, S.J. and Y.L. (Yangyang Liu); writing—original draft preparation, Z.Z.; writing—review and editing, B.Z.; supervision, L.Z. and X.F.; funding acquisition, D.W. and Z.X. All authors have read and agreed to the published version of the manuscript.

Funding: This research was funded by National Key Research and Development Program of China, grant number 2019YFA0705201.

Informed Consent Statement: Not applicable.

Data Availability Statement: The data presented in this study are available on request from the corresponding author.

Conflicts of Interest: The authors declare no conflict of interest.

References

1. Bartels, R.A.; Paul, A.; Green, H.; Kapteyn, H.C.; Murnane, M.M.; Backus, S.; Christov, I.P.; Liu, Y.; Attwood, D.; Jacobsen, C. Generation of spatially coherent light at extreme ultraviolet wavelengths. *Science* **2002**, *297*, 376–378. [[CrossRef](#)]
2. Huo, N.J.; Konstantatos, G. Recent progress and future prospects of 2d-based photodetectors. *Adv. Mater.* **2018**, *30*, 1801164. [[CrossRef](#)]
3. Pospischil, A.; Humer, M.; Furchi, M.M.; Bachmann, D.; Guider, R.; Fromherz, T.; Mueller, T. CMOS-compatible graphene photodetector covering all optical communication bands. *Nat. Photonics* **2013**, *7*, 892–896. [[CrossRef](#)]
4. Formisano, V.; Atreya, S.; Encrenaz, T.; Ignatiev, N.; Giuranna, M. Detection of methane in the atmosphere of Mars. *Science* **2004**, *306*, 1758–1761. [[CrossRef](#)]
5. Liu, W.B.; Zhang, J.F.; Zhu, Z.H.; Yuan, X.D.; Qin, S.Q. Electrically tunable absorption enhancement with spectral and polarization selectivity through graphene plasmonic light trapping. *Nanomaterials* **2016**, *6*, 155. [[CrossRef](#)] [[PubMed](#)]
6. Li, Y.F.; Zhang, Y.T.; Li, T.T.; Li, M.Y.; Chen, Z.L.; Li, Q.Y.; Zhao, H.L.; Sheng, Q.; Shi, W.; Yao, J. Ultrabroadband, ultraviolet to terahertz, and high sensitivity CH₃NH₃PbI₃ perovskite photodetectors. *Nano Lett.* **2020**, *20*, 5646–5654. [[CrossRef](#)]
7. Aldabahi, A.; Velazquez, R.; Zhou, A.F.; Rahaman, M.; Feng, P.X. Bandgap-tuned 2d boron nitride/tungsten nitride nanocomposites for development of high-performance deep ultraviolet selective photodetectors. *Nanomaterials* **2020**, *10*, 1433. [[CrossRef](#)] [[PubMed](#)]
8. Ni, S.M.; Guo, F.Y.; Wang, D.B.; Liu, G.; Xu, Z.K.; Kong, L.P.; Wang, J.Z.; Jiao, S.J.; Zhang, Y.; Yu, Q.J.; et al. Effect of MgO surface modification on the TiO₂ nanowires electrode for self-powered UV photodetectors. *ACS Sustain. Chem. Eng.* **2018**, *6*, 7265–7272. [[CrossRef](#)]
9. Liang, S.; Sheng, H.; Liu, Y.; Huo, Z.; Lu, Y.; Shen, H. ZnO Schottky ultraviolet photodetectors. *J. Cryst. Growth* **2001**, *225*, 110–113. [[CrossRef](#)]
10. Jiao, S.J.; Zhang, Z.Z.; Lu, Y.M.; Shen, D.Z.; Yao, B.; Zhang, J.Y.; Li, B.H.; Zhao, D.X.; Fan, X.W.; Tang, Z.K. ZnO p-n junction light-emitting diodes fabricated on sapphire substrates. *Appl. Phys. Lett.* **2006**, *88*, 031911. [[CrossRef](#)]
11. Monroy, E.; Omnes, F.; Calle, F. Wide-bandgap semiconductor ultraviolet photodetectors. *Semicond. Sci. Technol.* **2003**, *18*, R33–R51. [[CrossRef](#)]
12. Jin, Y.Z.; Wang, J.P.; Sun, B.Q.; Blakesley, J.C.; Greenham, N.C. Solution-processed ultraviolet photodetectors based on colloidal ZnO nanoparticles. *Nano Lett.* **2008**, *8*, 1649–1653. [[CrossRef](#)]
13. Gedamu, D.; Paulowicz, I.; Kaps, S.; Lupan, O.; Wille, S.; Haidarschin, G.; Mishra, Y.K.; Adelung, R. Rapid fabrication technique for interpenetrated ZnO nanotetrapod networks for Fast UV sensors. *Adv. Mater.* **2014**, *26*, 1541–1550. [[CrossRef](#)] [[PubMed](#)]
14. Hu, L.F.; Yan, J.; Liao, M.Y.; Xiang, H.J.; Gong, X.G.; Zhang, L.D.; Fang, X.S. An optimized ultraviolet-a light photodetector with wide-range photoresponse based on ZnS/ZnO biaxial nanobelt. *Adv. Mater.* **2012**, *24*, 2305–2309. [[CrossRef](#)]
15. Zhang, B.K.; Li, Q.; Wang, D.B.; Wang, J.Z.; Jiang, B.J.; Jiao, S.J.; Liu, D.H.; Zeng, Z.; Zhao, C.C.; Liu, Y.X.; et al. Efficient photocatalytic hydrogen evolution over TiO_{2-x} mesoporous spheres-ZnO nanowires heterojunction. *Nanomaterials* **2020**, *10*, 2096. [[CrossRef](#)]
16. Liu, X.; Gu, L.L.; Zhang, Q.P.; Wu, J.Y.; Long, Y.Z.; Fan, Z.Y. All-printable band-edge modulated ZnO nanowire photodetectors with ultra-high detectivity. *Nat. Commun.* **2014**, *5*, 1–9. [[CrossRef](#)] [[PubMed](#)]

17. Kim, H.; Yan, H.Q.; Messer, B.; Law, M.; Yang, P.D. Nanowire ultraviolet photodetectors and optical switches. *Adv. Mater.* **2002**, *14*, 158–160.
18. Yang, J.L.; Liu, K.W.; Shen, D.Z. Recent progress of ZnMgO ultraviolet photodetector. *Chin. Phys. B* **2017**, *26*, 047308. [[CrossRef](#)]
19. Gu, P.; Zhu, X.H.; Yang, D.Y. Vertically aligned ZnO nanorods arrays grown by chemical bath deposition for ultraviolet photodetectors with high response performance. *J. Alloys Compd.* **2020**, *815*, 152346. [[CrossRef](#)]
20. Park, Y.H.; Shin, H.; Noh, S.J.; Kim, Y.; Lee, S.S.; Kim, C.G.; An, K.S.; Park, C.Y. Optical quenching of NiO/Ni coated ZnO nanowires. *Appl. Phys. Lett.* **2007**, *91*, 012102. [[CrossRef](#)]
21. Liu, S.; Liao, Q.L.; Zhang, Z.; Zhang, X.K.; Lu, S.N.; Zhou, L.X.; Hong, M.Y.; Kang, Z.; Zhang, Y. Strain modulation on graphene/ZnO nanowire mixed dimensional van der Waals heterostructure for high-performance photosensor. *Nano Res.* **2017**, *10*, 3476–3485. [[CrossRef](#)]
22. Li, C.L.; Han, C.; Zhang, Y.B.; Zang, Z.G.; Wang, M.; Tang, X.S.; Du, J.H. Enhanced photoresponse of self-powered perovskite photodetector based on ZnO nanoparticles decorated CsPbBr₃ films. *Sol. Energy. Mat. Sol. Cells* **2017**, *172*, 341–346. [[CrossRef](#)]
23. Patel, M.; Pataniya, P.M.; Patel, V.; Sumesh, C.K.; Late, D.J. Large area, broadband and highly sensitive photodetector based on ZnO-WS₂/Si heterojunction. *Sol. Energy* **2020**, *206*, 974–982. [[CrossRef](#)]
24. Hsiao, Y.J.; Fang, T.H.; Ji, L.W.; Yang, B.Y. Red-shift effect and sensitive responsivity of MoS₂/ZnO flexible photodetectors. *Nanoscale Res. Lett.* **2015**, *10*, 443. [[CrossRef](#)]
25. Oh, I.K.; Kim, W.H.; Zeng, L.; Singh, J.; Bae, D.; Mackus, A.J.M.; Song, J.G.; Seo, S.; Shong, B.; Kim, H.; et al. Synthesis of a hybrid nanostructure of ZnO-decorated MoS₂ by atomic layer deposition. *ACS Nano* **2020**, *14*, 1757–1769. [[CrossRef](#)] [[PubMed](#)]
26. Lan, C.Y.; Li, C.; Wang, S.; Yin, Y.; Guo, H.Y.; Liu, N.S.; Liu, Y. ZnO-WS₂ heterostructures for enhanced ultra-violet photodetectors. *RSC Adv.* **2016**, *6*, 67520–67524. [[CrossRef](#)]
27. Lv, W.Q.; Liu, J.; He, Y.; You, J.H. Atomic layer deposition of ZnO thin film on surface modified monolayer MoS₂ with enhanced photoresponse. *Ceram. Int.* **2018**, *44*, 23310–23314. [[CrossRef](#)]
28. Ma, J.C.; Deng, K.; Zheng, L.; Wu, S.F.; Liu, Z.; Zhou, S.Y.; Sun, D. Experimental progress on layered topological semimetals. *2D Mater.* **2019**, *6*, 032001. [[CrossRef](#)]
29. Lai, J.W.; Liu, X.; Ma, J.C.; Wang, Q.S.; Zhang, K.N.; Ren, X.; Liu, Y.N.; Gu, Q.Q.; Zhuo, X.; Lu, W.; et al. Anisotropic broadband photoresponse of layered Type-II weyl semimetal MoTe₂. *Adv. Mater.* **2018**, *30*, 1707152. [[CrossRef](#)] [[PubMed](#)]
30. Zeng, Z.; Wang, D.B.; Wang, J.Z.; Jiao, S.J.; Huang, Y.W.; Zhao, S.X.; Zhang, B.K.; Ma, M.Y.; Gao, S.Y.; Feng, X.; et al. Self-assembly synthesis of the MoS₂/PtCo alloy counter electrodes for high-efficiency and stable low-cost dye-sensitized solar cells. *Nanomaterials* **2020**, *10*, 1725. [[CrossRef](#)] [[PubMed](#)]
31. Zeng, L.H.; Lin, S.H.; Li, Z.J.; Zhang, Z.X.; Zhang, T.F.; Xie, C.; Mak, C.H.; Chai, Y.; Lau, S.P.; Luo, L.B.; et al. Driven, air-stable, and broadband photodetector based on vertically aligned PtSe₂/GaAs heterojunction. *Adv. Funct. Mater.* **2018**, *28*, 1705970. [[CrossRef](#)]
32. Lee, Y.F.; Punugupati, S.; Wu, F.; Jin, Z.; Narayan, J.; Schwartz, J. Evidence for topological surface states in epitaxial Bi₂Se₃ thin film grown by pulsed laser deposition through magneto-transport measurements. *Curr. Opin. Solid State Mater. Sci.* **2014**, *18*, 279–285. [[CrossRef](#)]
33. Yu, X.C.; Yu, P.; Wu, D.; Singh, B.; Zeng, Q.S.; Lin, H.; Zhou, W.; Lin, J.H.; Suenaga, K.; Liu, Z.; et al. Atomically thin noble metal dichalcogenide: A broadband mid-infrared semiconductor. *Nat. Commun.* **2018**, *9*, 1–9. [[CrossRef](#)]
34. Yin, J.B.; Tan, Z.J.; Hong, H.; Wu, J.X.; Yuan, H.T.; Liu, Y.J.; Chen, C.; Tan, C.W.; Yao, F.R.; Li, T.R.; et al. Ultrafast and highly sensitive infrared photodetectors based on two-dimensional oxyselenide crystals. *Nat. Commun.* **2018**, *9*, 3311. [[CrossRef](#)] [[PubMed](#)]
35. Wang, D.B.; Jiao, S.J.; Sun, S.J.; Zhao, L.C. Al_{0.40}In_{0.58}N Based Metal-semiconductor-metal Photodiodes for Ultraviolet Detection. In Proceedings of the 2012 International Conference on Optoelectronics and Microelectronics, Changchun, China, 23–25 August 2012.
36. Zhang, X.; Zhu, T.S.; Huang, J.W.; Wang, Q.; Cong, X.; Bi, X.Y.; Tang, M.; Zhang, C.R.; Zhou, L.; Zhang, D.Q.; et al. Electric field tuning of interlayer coupling in noncentrosymmetric 3R-MoS₂ with an electric double layer interface. *ACS Appl. Mater. Interfaces* **2020**, *12*, 46900–46907. [[CrossRef](#)] [[PubMed](#)]
37. Lim, H.; Lee, J.S.; Shin, H.J.; Shin, H.S.; Choi, H.C. Spatially resolved spontaneous reactivity of diazonium salt on edge and basal plane of graphene without surfactant and its doping effect. *Langmuir* **2010**, *26*, 12278–12284. [[CrossRef](#)]
38. Ayalakshmi, G.; Saravanan, K. High-performance UV surface photodetector based on plasmonic Ni nanoparticles-decorated hexagonal-faceted ZnO nanorod arrays architecture. *J. Mater. Sci. Mater. Electron.* **2020**, *31*, 5710–5720. [[CrossRef](#)]
39. Cheng, H.M.; Hsu, H.C.; Tseng, Y.K.; Lin, L.J.; Hsieh, W.F. Scattering and efficient UV photoluminescence from well-aligned ZnO nanowires epitaxially grown on gan buffer layer. *J. Phys. Chem. B* **2005**, *109*, 8749–8754. [[CrossRef](#)]
40. Liu, G.; Kong, L.P.; Hu, Q.Y.; Zhang, S.J. Diffused morphotropic phase boundary in relaxor-PbTiO₃ crystals: High piezoelectricity with improved thermal stability. *Appl. Phys. Rev.* **2020**, *7*, 021405. [[CrossRef](#)]
41. Zhang, J.; Peng, Z.P.; Soni, A.; Zhao, Y.Y.; Xiong, Y.; Peng, B.; Wang, J.B.; Dresselhaus, M.S.; Xiong, Q.H. Raman spectroscopy of few-quintuple layer topological insulator Bi₂Se₃ nanoplatelets. *Nano Lett.* **2011**, *11*, 2407–2414. [[CrossRef](#)] [[PubMed](#)]
42. Buchenau, S.; Scheitz, S.; Sethi, A.; Slimak, J.E.; Glier, T.E.; Das, P.K.; Dankwort, T.; Akinsinde, L.; Kienle, L.; Rusydi, A.; et al. Temperature and magnetic field dependent Raman study of electron-phonon interactions in thin films of Bi₂Se₃ and Bi₂Te₃ nanoflakes. *Phys. Rev. B* **2020**, *101*, 245431. [[CrossRef](#)]

43. Liu, B.; Liao, Q.L.; Zhang, X.K.; Du, J.L.; Ou, Y.; Xiao, J.K.; Kang, Z.; Zhang, Z.; Zhang, Y. Strain-engineered van der Waals interfaces of mixed-dimensional heterostructure arrays. *ACS Nano* **2019**, *13*, 9057–9066. [[CrossRef](#)] [[PubMed](#)]
44. Lloyd, D.; Liu, X.; Christopher, J.W.; Cantley, L.; Wadehra, A.; Kim, B.L.; Goldberg, B.B.; Swan, A.K.; Bunch, J.S. Band gap engineering with ultralarge biaxial strains in suspended monolayer MoS₂. *Nano Lett.* **2016**, *16*, 5836–5841. [[CrossRef](#)]
45. Alwadai, N.; Ajia, I.A.; Janjua, B.; Flemban, T.H.; Mitra, S.; Wehbe, N.; Wei, N.N.; Lopatin, S.; Ooi, B.S.; Roqan, I.S. Catalyst-free vertical ZnO-nanotube array grown on p-GaN for UV-light-emitting devices. *ACS Appl. Mater. Interfaces* **2019**, *11*, 27989–27996. [[CrossRef](#)]
46. Djuricic, A.B.; Leung, Y.H. Optical properties of ZnO nanostructures. *Small* **2006**, *2*, 944–961. [[CrossRef](#)]
47. Bohle, D.S.; Spina, C.J. The relationship of oxygen binding and peroxide sites and the fluorescent properties of zinc oxide Semiconductor nanocrystals. *J. Am. Chem. Soc.* **2007**, *129*, 12380–12381. [[CrossRef](#)]
48. Stroyuk, O.L.; Dzhagan, V.M.; Shvalagin, V.V.; Kuchmiy, S.Y. Size-dependent optical properties of colloidal ZnO nanoparticles charged by photoexcitation. *J. Phys. Chem. C* **2010**, *114*, 220–225. [[CrossRef](#)]
49. Zhang, H.B.; Zhang, X.J.; Liu, C.; Lee, S.T.; Jie, J.S. High-responsivity, high-detectivity, ultrafast topological insulator Bi₂Se₃/silicon heterostructure broadband photodetectors. *ACS Nano* **2016**, *10*, 5113–5122. [[CrossRef](#)] [[PubMed](#)]
50. Liu, C.; Zhang, H.B.; Sun, Z.; Ding, K.; Mao, J.; Shao, Z.B.; Jie, J.S. Topological insulator Bi₂Se₃ nanowire/Si heterostructure photodetectors with ultrahigh responsivity and broadband response. *J. Phys. Chem. C* **2016**, *4*, 5648–5655.
51. Wang, X.; Wu, H.; Wang, G.; Ma, X.; Xu, Y.; Zhang, H.; Jin, L.; Shi, L.; Zou, Y.; Yin, J.; et al. Study of the optoelectronic properties of ultraviolet photodetectors based on Zn-Doped CuGaO₂ Nanoplate/ZnO nanowire heterojunctions. *Phys. Status Solidi* **2020**, *257*, 1900684. [[CrossRef](#)]
52. Zhu, Y.X.; Liu, K.W.; Wang, X.; Yang, J.L.; Chen, X.; Xie, X.H.; Li, B.H.; Shen, D.Z. Performance improvement of a ZnMgO ultraviolet detector by chemical treatment with hydrogen peroxide. *J. Mater. Chem. C* **2017**, *5*, 7598–7603. [[CrossRef](#)]
53. Chen, X.; Liu, K.W.; Wang, X.; Li, B.H.; Zhang, Z.Z.; Xie, X.H.; Shen, D.Z. Performance enhancement of a ZnMgO film UV photodetector by HF solution treatment. *J. Mater. Chem. C* **2017**, *5*, 10645–10651. [[CrossRef](#)]
54. Nasiri, N.; Bo, R.; Hung, T.F.; Roy, V.A.L.; Fu, L.; Tricoli, A. Tunable band-selective UV-photodetectors by 3D Self-assembly of heterogeneous nanoparticle networks. *Adv. Funct. Mater.* **2016**, *26*, 7359–7366. [[CrossRef](#)]
55. Ismail, R.A.; Al-Naimi, A.; Al-Ani, A.A. Studies on fabrication and characterization of a high-performance Al-doped ZnO/n-Si (111) heterojunction photodetector. *Semicond. Sci. Technol.* **2008**, *23*, 075030. [[CrossRef](#)]
56. Ali, A.; Wang, D.B.; Wang, J.Z.; Jiao, S.J.; Guo, F.Y.; Zhang, Y.; Gao, S.Y.; Ni, S.M.; Luan, C.; Wang, D.Z.; et al. ZnO nanorod arrays grown on an AlN buffer layer and their enhanced ultraviolet emission. *CrystEngComm* **2017**, *19*, 6085–6088. [[CrossRef](#)]
57. Sun, X.W.; Huang, J.Z.; Wang, J.X.; Xu, Z. A ZnO nanorod inorganic/organic heterostructure light-emitting diode emitting at 342 nm. *Nano Lett.* **2008**, *8*, 1219–1223. [[CrossRef](#)] [[PubMed](#)]
58. Gupta, A.; Chowdhury, R.K.; Ray, S.K.; Srivastava, S.K. Selective photoresponse of plasmonic silver nanoparticle decorated Bi₂Se₃ nanosheets. *Nanotechnology* **2019**, *30*, 435204. [[CrossRef](#)]